

A critical assessment of theories of strain gradient plasticity

A.G. Evans^{a,b}, J.W. Hutchinson^{c,*}

^a Department of Materials Engineering, University of California, Santa Barbara, CA 93106, USA

^b Department of Mechanical Engineering, University of California, Santa Barbara, CA 93106, USA

^c School of Engineering and Applied Sciences, Harvard University, Cambridge, MA 02138, USA

Received 20 August 2008; received in revised form 4 December 2008; accepted 6 December 2008

Available online 6 January 2009

Abstract

Theories to extend plasticity to the micron scale have been in existence for over a decade, complemented by a growing body of experimental data. Here, materials and mechanics aspects of two prominent strain gradient theories of plasticity, due to Nix and Gao and to Fleck and Hutchinson, are assessed within the context of simple bending. Differences between the theories are highlighted. The theories predict different trends relative to the size dependence of initial yielding and rate of hardening. The dislocation mechanics underpinning the two theories is addressed. Distinctions between lower-order theories and higher-order theories are also drawn, emphasizing the flexibility of higher-order theories to solve problems for a wide range of boundary conditions, especially those where, locally, the dislocations are blocked (pile up) and the plastic strain is zero.

© 2008 Acta Materialia Inc. Published by Elsevier Ltd. All rights reserved.

Keywords: Plasticity; Size effects; Geometrically necessary dislocations; Bending

1. Introduction

The elevation of the plastic flow stress in small volumes is well documented [1–11]. The effects of configuration size have been presented for indentation [1–6], torsion [7], bending and thin film extension [8,9]. Microstructural size effects include those due to grain boundaries (Hall–Petch) [10] and particle reinforcements [11]. In all these cases, strain gradients are involved and, in such instances, there is general agreement that the size effect, which generally manifests itself at the micron scale, can be attributed to hardening enabled by geometrically necessary dislocations (GND) [12]. The constitutive laws that ensue include a contribution from the uniform plastic strain ε_p , and another incorporating a length scale ℓ , in conjunction with a plastic strain gradient $\varepsilon_p^* \equiv |d\varepsilon_p/dx|$. The uniform strain is associated with the statistically stored dislocations (SSD), density ρ_{SSD} , and the gradient with the GND, density ρ_{GND} [7]. To

establish a viable computational scheme, these contributions must be combined in an appropriate manner. Almost 25 years after the introduction of the first theory of strain gradient plasticity (SGP) [13], and following a decade of active research into small-scale plasticity, the aim of the present paper is to provide a critical assessment from the vantage points of both mechanics and materials science by delving into two basic approaches to combining the strain and its gradient. One theory developed by Fleck and Hutchinson [14,15] (FH) is based on plastic dissipation and considers separate, additive contributions from the SSD and GND. Another, introduced by Nix and Gao [4,16–18] (NG), invokes an enhanced flow stress governed by the density of the GND. Both formulations have the following commonalities: (i) they are phenomenological in that they employ isotropic measures of the plastic strain and its gradient; (ii) they aspire to extend the classical J_2 theory of plasticity in the simplest meaningful manner into the range where size dependence becomes important; (iii) they reduce to J_2 theory when the scale of the gradient is large compared with ℓ . Nevertheless, they predict different trends in the flow stress. The distinctions between them will

* Corresponding author. Tel.: +1 617 495 2848; fax: +1 617 496 0601.
E-mail address: hutchinson@husm.harvard.edu (J.W. Hutchinson).

be highlighted in the present paper by comparing and contrasting predictions for an especially straightforward loading situation, described below. Thereafter, the merits and limitations of the theories will be discussed and alternative suggestions made.

The distinctions between the theories are most clearly revealed by bending, because the total strain gradient is spatially constant, inducing both SSD and GND as soon as plastic flow commences. Data for the bending moment induced in Ni foils as a function of curvature are used (Fig. 1) [19]. Details of the experiments are given elsewhere [19]. The principle of the test design is to bend a thin foil to a prescribed curvature. When unloaded, the foil relaxes elastically to a smaller, permanent curvature. The decrease in curvature upon unloading provides a measure of the bending moment per width M , without requiring independent measurement. The results of the bending measurements conducted for foils of thickness h are presented as plots of the normalized bending moment M/h^2 , as a function the surface strain, $\varepsilon_S = \kappa h/2$ and in terms of the reduced surface strain, defined as the difference between the surface strain and the surface strain due to M for elastic bending: $\varepsilon_S^R = \varepsilon_S - 6(1 - \nu^2)M/(Eh^2)$. (The elastic strain contribution

is of no significance for present purposes.) The normalization used in these plots would collapse the data onto a single curve in the absence of a material size effect. The results are presented in a manner that highlights the separate dependences on foil thickness and grain size. Those summarized in Fig. 1a and c are for foils with the same grain size ($g = 27 \mu\text{m}$) but differing thickness (10, 50 and 125 μm), revealing the increase in flow stress with decrease in thickness at a fixed grain size. The corresponding results in Fig. 1b and d are all for foils with the same thickness ($h = 50 \mu\text{m}$) but three grain sizes (6, 14, and 27 μm). The increase in flow stress with decrease in grain size is evident. Tensile stress/plastic strain curves representative of those for polycrystalline Ni at the four different grain sizes are presented in Fig. 2 [19–21]. These measurements will be assessed in the context of the NG and FH theories.

In order to bring out differences between the theories, two additional sets of measurements are invoked (Fig. 3). One comprises the series of torsion tests conducted on Cu wires of different diameter [7]. Note the strong influence of the diameter on the yield strength, but relatively small effect on the strain hardening. The other is the comparison between the tensile response of thin foils with and without

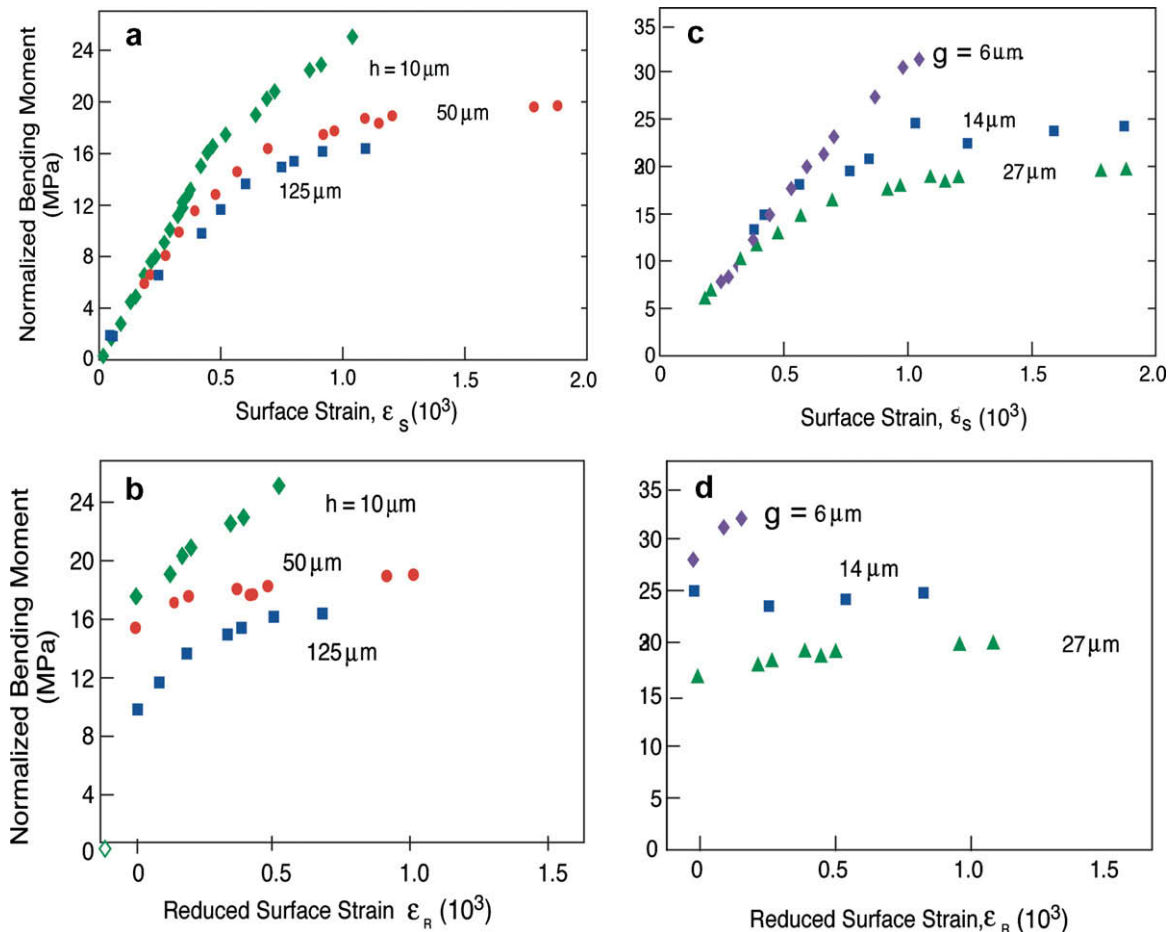


Fig. 1. Normalized moment M/h^2 as a function of surface strain ε_S and reduced surface strain ε_R for Ni foils: (a and b) for three thicknesses with grain size $g = 27 \mu\text{m}$; (c and d) for three grain sizes with foil thickness $h = 50 \mu\text{m}$ [19].

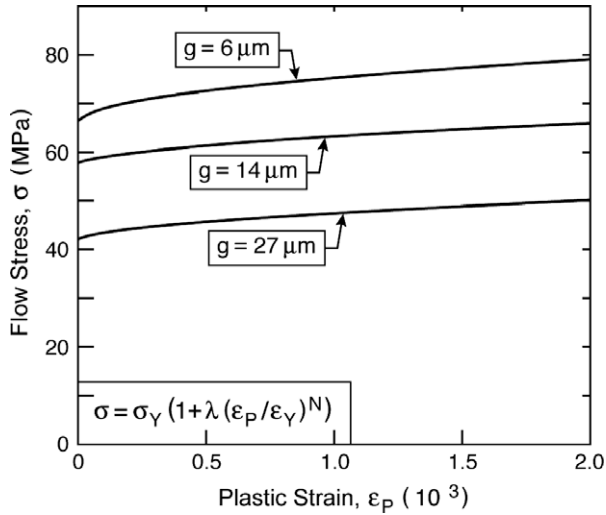


Fig. 2. Tensile stress–plastic strain data for foils with three grain sizes [19–21].

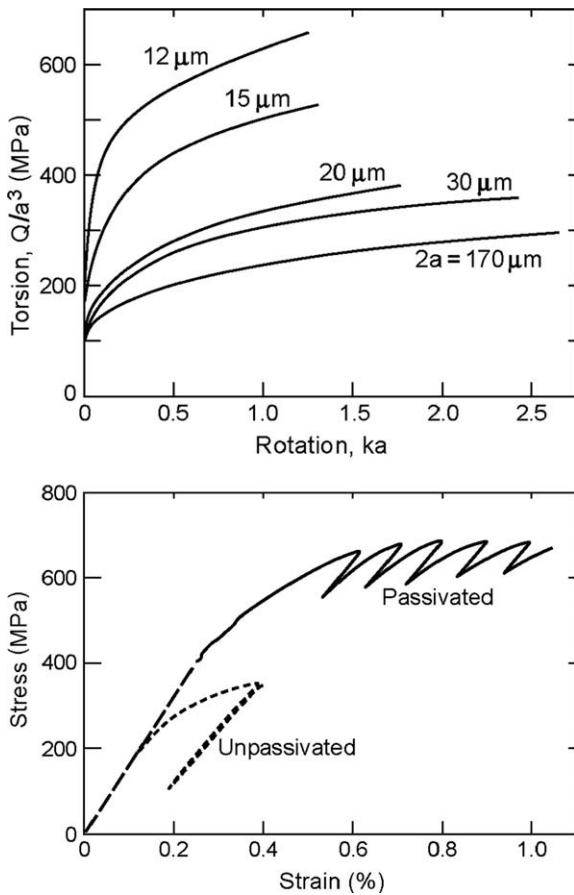


Fig. 3. Upper plot: normalized torque vs normalized rotation for copper wires of various radius a [7]. This normalization would collapse the data to a single curve if there were no material size dependence. Lower plot: tensile stress–strain data for thin copper films ($0.34 \mu\text{m}$) that are unpassivated and passivated (on one surface) [9].

a passivated surface layer [9]. The presence of the passivated layer also increases the yield strength, with a much smaller effect on the strain hardening.

The present assessment continues that initiated by Nix and Gao [4] by focusing on the fidelity and underpinnings of the simplest generalizations of conventional plasticity. It also emphasizes the distinction between lower- and higher-order gradient plasticity theories, to make the point that only the latter is capable of solving important categories of problem, such as those involving dislocation pile ups. The unresolved issues it does not attempt to address are as follows: (i) details of the higher-order formulations and the full scope of the boundary conditions to which these apply [22,23]; (ii) the partitioning of the plastic work due to strain gradients into dissipative and recoverable contributions under highly non-proportional multiaxial stressing [24] (not at issue for pure bending); (iii) single crystal formulations of SGP, whether cast within a continuum framework [25,26] or based on discrete dislocations [27].

The paper is organized as follows. Basic aspects of plasticity relevant to gradient effects are presented, the two formulations are described and general trends elucidated. Thereafter, the predictions of the theories for bending are compared with the measurements, enabling conclusions to be reached about their respective merits and deficiencies. Finally, the discussion is broadened by introducing other measurements that support the conclusions and by clarifying the scaling, as well as the connection to dislocation-based concepts of hardening.

2. The interaction of plastic strains and strain gradients

2.1. Focus

The focus is on the manner whereby the plastic strains and their gradients are combined in the SGP theories. Issues related to the pertinence of lower- or higher-order theories (Appendix A) do not explicitly affect the bending assessment. However, because the distinction is crucially important for certain classes of problems, one example requiring the higher-order formulation is given in Section 4. The simpler deformation (rather than incremental) theories of plasticity are used, consistent with the bending moments being measured at increasing curvature (Fig. 1), involving monotonic plane strain tension or compression.

2.2. Definitions

The effective stress and plastic strain are, respectively, $\sigma_e = \sqrt{3s_{ij}s_{ij}/2}$ and $\epsilon_p = \sqrt{2\epsilon_{ij}^p\epsilon_{ij}^p/3}$, with ϵ_{ij}^p the plastic strain tensor, and s_{ij} the stress deviator. In uniaxial tension, σ_e and ϵ_p coincide with the stress and the plastic strain, respectively, and the uniaxial stress–strain curve is characterized by function f according to $\sigma_e = \sigma_Y f(\epsilon_p)$, with σ_Y the yield strength. This relation holds for proportional multiaxial stressing in the absence of gradients. The associated plastic work/volume is

$$U_P(\epsilon_p) = \sigma_Y \int_0^{\epsilon_p} f(\epsilon_p) d\epsilon_p \quad (1)$$

2.3. The theories

The two theories each provide a length scale, designated ℓ_{NG} and ℓ_{FH} for Nix/Gao and Fleck/Hutchinson, respectively. Definitions for these lengths, within the context of the theories, will be provided in this section (see also Appendix A). The interpretation of the lengths in terms of the governing dislocation phenomena will be deferred to Section 6. The theory introduced by Nix et al. [4,16] is inspired by Taylor hardening, with flow stress governed by the interaction of the mobile dislocations with the SSD and GND, through a linear summation of their densities, $\sigma_e \sim Gb\sqrt{\rho_{\text{SSD}} + \rho_{\text{GND}}}$, where G is the shear modulus, and b the Burgers vector. Interactions between the SSD and GND are not considered. The theory is expressed as a gradient-enhanced flow stress:

$$\sigma_e = \sqrt{[\sigma_Y f(\varepsilon_P)]^2 + \chi \alpha^2 G^2 b \varepsilon_P^*} \quad (2)$$

Here, ε_P^* is the magnitude of the gradient of plastic strain, $\chi = m^2 \bar{r} \cong 18$, with m the Taylor factor connecting the tensile yield stress of a polycrystal with the single crystal shear yield stress ($m = 3.06$ for FCC), and $\bar{r} \cong 1.85$ the Nye factor. The Taylor hardening coefficient α is regarded as a constant, expected to be in the range $0.2 < \alpha < 0.4$. In the implementation of the NG theory, it has been treated as a fitting parameter. The first term in Eq. (2) is attributed to the SSD and reproduces uniaxial tension data. The second is associated with the GND, as discussed further in Section 6. The length parameter ℓ_{NG} is defined by

$$\ell_{\text{NG}} = \chi \left(\frac{G}{\sigma_Y} \right)^2 \alpha^2 b \quad (3)$$

such that

$$\sigma_e = \sigma_Y \sqrt{(f(\varepsilon_P))^2 + \ell_{\text{NG}} \varepsilon_P^*} \quad (4)$$

Both ℓ_{NG} and α will be presented when fitting the NG theory to data.

The premise of the FH [14,15] theory is that the movement of the SSD and GND results in plastic dissipation governed by an effective plastic strain E_P , re-expressed from (1) as

$$U_P(E_P) = \sigma_Y \int_0^{E_P} f(\varepsilon_P) d\varepsilon_P \quad (5)$$

In the ensuing assessment, the preferred measure of E_P is the linear summation

$$E_P = \varepsilon_P + \ell_{\text{FH}} \varepsilon_P^* \quad (6)$$

with ℓ_{FH} the associated material length parameter. The first term provides the plastic dissipation caused by the motion of the SSD, and the second term that attributed to the GND. This choice reduces to classical theory in the limit when gradients are small, with $E_P \cong \varepsilon_P$. (More generally, E_P has been prescribed by the homogeneous composition

$$E_P = (\varepsilon_P^\mu + (\ell_{\text{FH}} \varepsilon_P^*)^\mu)^{1/\mu} \quad (7)$$

The version with $\mu = 2$ has been employed in most studies using FH theory. For reasons elaborated below and in Appendix B, the linear summation with $\mu = 1$ is more attractive and will be used hereafter.)

2.4. General trends

General trends can be revealed by considering the non-uniform deformations of an object, size h , which experiences average plastic strain ε_P and average strain gradient $\varepsilon_P^* = c\varepsilon_P/h$ (where $c \approx 1$). Trends are revealed most clearly for a perfectly plastic solid, with $f(\varepsilon_P) = 1$. Upon approximating the average of the square root by the square root of the average, the NG formulation predicts an average flow stress

$$\sigma \approx \sigma_Y \sqrt{1 + (c\ell_{\text{NG}}/h)\varepsilon_P} \quad (8)$$

plotted in Fig. 4b for various h . Note that strain gradients do not elevate the yield strength. Instead, they increase the rate of strain hardening. Moreover, the gradient effect only becomes important when $(c\ell_{\text{NG}}/h)\varepsilon_P$ is of order unity. By invoking a similar approximation, the corresponding trends for the FH formulation are

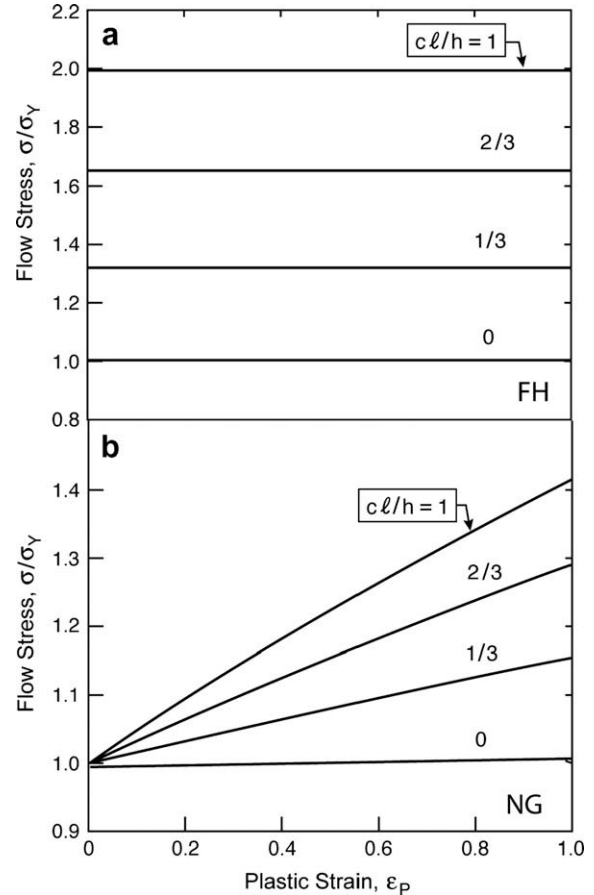


Fig. 4. Trends of average flow stress as a function of average plastic strain ε_P for an object of size h subject to an average gradient of plastic strain $\varepsilon_P^* = c\varepsilon_P/h$: (a) FH; (b) NG formulations.

$$E_p \approx [1 + (c\ell_{FH}/h)]\varepsilon_p \quad (9)$$

and

$$U_p(E_p) = \sigma_Y [1 + (c\ell_{FH}/h)]\varepsilon_p \quad (10)$$

with average flow stress

$$\sigma \approx \sigma_Y [1 + (c\ell_{FH}/h)] \quad (11)$$

In this formulation (Fig. 4a), the gradient elevates the yield strength but not the rate of hardening. Moreover, the flow stress increases linearly with $c\ell_{FH}/h$ independent of ε_p .

The foregoing distinction is persistent and represents one of the major differentiators between the formulations, i.e., the NG formulation increases the hardening rate, but not the yield strength, while FH formulation increases the yield strength, with a second-order influence on hardening.

3. Application to pure bending

The size dependence of the moment–curvatures relation in pure bending will be explored using the NG and FH models. The tensile stress–strain data for the Ni foils (Fig. 2) over the range of interest can be represented by

$$\begin{aligned} \sigma &= E\varepsilon (\varepsilon_p = 0), \quad \sigma \leq \sigma_Y \\ \sigma &= \sigma_Y [1 + \lambda(\varepsilon_p/\varepsilon_Y)^N], \quad \sigma > \sigma_Y \end{aligned} \quad (12)$$

where $\varepsilon_Y = \sigma_Y/E$ is the yield strain. The parameters σ_Y , λ and N are chosen to fit data for each grain size (Table 1). Elasticity will be taken to be isotropic with Young’s modulus $E = 220$ GPa. To simplify the analysis, elastic compressibility will be neglected by taking Poisson’s ratio as 1/2, with little effect on the results of interest in the plastic range. The only other input is the material length scale. For each model, this will be chosen to fit the data.

The bending data are restricted to small strains, justifying the use of linear strain–displacement theory. In pure bending, the strain variation across the cross-section is $\varepsilon_{11} \equiv \varepsilon = \kappa y$, with κ the imposed curvature, and y the distance from the mid-plane. For plane strain with elastic incompressibility, the effective plastic strain is related to the component parallel to the foil by

$$\varepsilon_p = 2|\varepsilon_{11}^p|/\sqrt{3} \quad (13)$$

The plastic strain distribution $\varepsilon_p(y)$ is the primary unknown in all the theories. The strain at the surface of a foil, thickness h , is $\varepsilon_S = \kappa h/2$. The curvature at which initial yield occurs at the surface in the conventional solid ($\ell = 0$) is $\kappa_Y = \sqrt{3}\varepsilon_Y/h$, and the associated moment/length is $M_Y = \sigma_Y h^2/(3\sqrt{3})$.

Table 1
Specification of uniaxial data.

Grain size g (μm)	σ_Y (MPa)	λ	N
6	66	0.078	0.49
14	57.5	0.043	0.60
27	42	0.050	0.57

3.1. Foils with fixed grain size ($g \cong 27 \mu\text{m}$) at three different thicknesses

Curves of moment against reduced surface strain based on the NG model are plotted in Fig. 5. Details of the calculations are given in Appendix A. The length parameter was chosen to fit the measurements for the foil with thickness $h = 50 \mu\text{m}$ (for which the data are most extensive) at $\varepsilon_S = 2 \times 10^{-3}$ ($\varepsilon_R \cong 1.6 \times 10^{-3}$, $\kappa/\kappa_Y = 10.5$, $M/h^2 \cong 20$ MPa). Thereafter, the same length is used to predict the remaining curves. To obtain a fit, a large length, $\ell_{NG} = 25$ mm, is required such that $\alpha = 1.13$. The corresponding fit plotted in Fig. 5 for the FH formulation requires a much smaller length parameter, $\ell_{FH} = 5 \mu\text{m}$ (computational details in Appendix A).

3.2. Foils with the same thickness ($h = 50 \mu\text{m}$) but different grain size (Fig. 6)

The analysis uses the input parameters summarized in Table 1, with the length parameters chosen independently

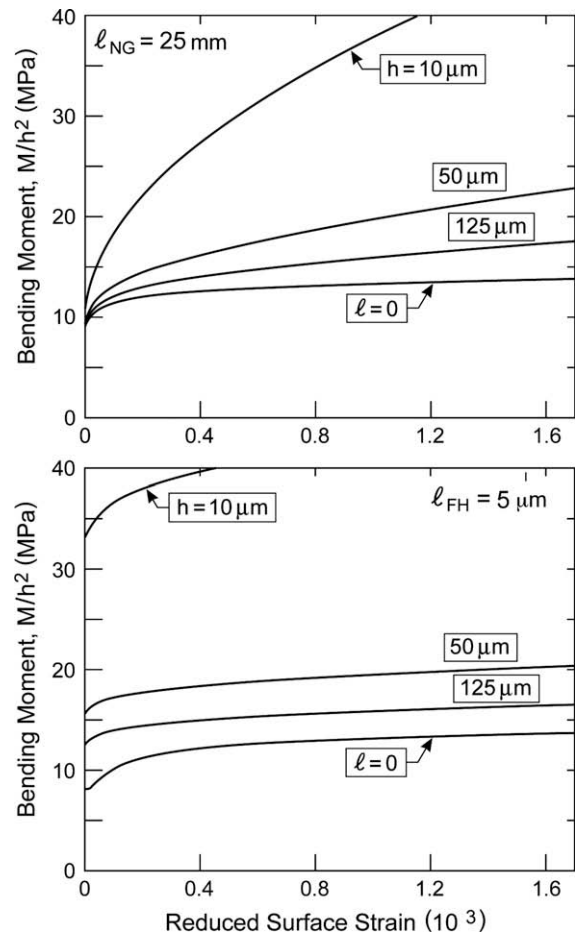


Fig. 5. Predictions of the normalized bending moment M/h^2 as a function of the reduced surface strain, $\varepsilon_S^R = \varepsilon_S - 6(1 - \nu^2)M/(Eh^2)$, for three foil thicknesses, all with grain size $g = 27 \mu\text{m}$. In each case, the length parameter was chosen to fit the experimental data in Fig. 1 for $h = 50 \mu\text{m}$. Upper plot, predictions of NG theory with $\ell_{NG} = 25$ mm ($\alpha = 1.13$); lower plot, predictions of FH theory ($\mu = 1$) with $\ell_{FH} = 5 \mu\text{m}$.

for each grain size to give the fit shown. Significantly, the length parameters (ℓ_{NG} and ℓ_{FH}) are only modestly dependent on grain size. The trends in Figs. 5 and 6 in flow stress and hardening elevation follow the pattern noted earlier.

The reason for the large ℓ_{NG} becomes apparent from Eq. (4) upon noting that, for the size effect to be appreciable, $\ell_{\text{NG}}\varepsilon_p^*$ must be comparable with $f(\varepsilon)$, which, in turn, is only slightly larger than unity, i.e., because the plastic strains are only of order 10^{-3} , the gradient is $\varepsilon_p^* \approx (10^{-3}/h)$, requiring $\ell_{\text{NG}} \approx 10^3 h$ for $\ell_{\text{NG}}\varepsilon_p^*$ to be comparable with unity. The existence of such large ℓ_{NG} is unprecedented and attributed to its strong strain dependence. All previous assessments have used stress data at much larger strains, inferring smaller ℓ_{NG} . Notably, results for the torsion of copper wires (Fig. 3) [17] twisted to surface strains of order unity gave ℓ_{NG} in the micron range, while indentation results (average strains typically 0.1) typically infer tens of microns [6]. The corresponding values of α are not constant. Instead, for torsion and some indentation data, it falls in the range 0.2–0.4 while, for bending, $\alpha = 1.13$. The implied strain dependence (while less than that for ℓ_{NG}) is thus apprecia-

ble, especially as the theory predicts an enhanced flow stress that varies as α^2 .

By contrast, ℓ_{FH} is in the micron range for all cases: small strain bending, large strain torsion and indentation. The FH formulation does not give rise to appreciable strain dependence for a given material because, in the definition of the effective plastic strain E_p , the plastic strain gradient is “balanced” against the plastic strain. In other words, the relative importance of the two contributions does not vary with the overall strain level.

The comparison of the predicted and measured moment/curvature curves in the plastic range (Figs. 7 and 8) reveals discrepancies for both models, notwithstanding that some of the deviations are associated with measurement fidelity at the smallest foil thickness, i.e., these measurements (together with those in Fig. 2) provide a clear indication of a yield strength elevation with thinness, at variance with NG. However, FH is also at variance with the bending measurements. It predicts (sometimes substantially) larger yield strength elevations and lower hardening rates than found experimentally. One implication is that both models, in their simplest (foregoing) manifestation,

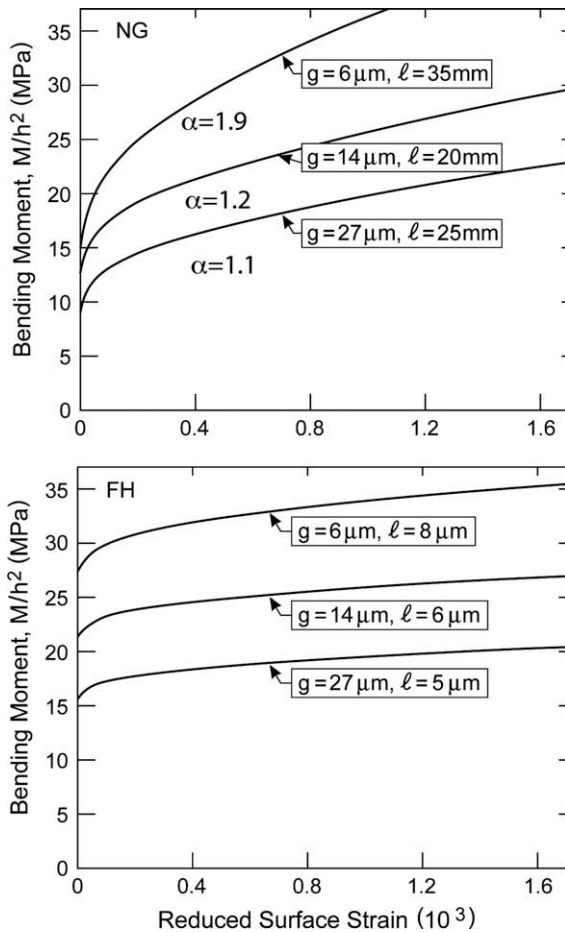


Fig. 6. Predictions of the normalized bending moment M/h^2 as a function of the reduced surface strain for three grain sizes all for foils with thickness $h = 50 \mu\text{m}$. In each case, the length parameter was chosen independently to give the best fit to the data in Fig. 1: upper figure, NG theory; lower figure, FH theory.

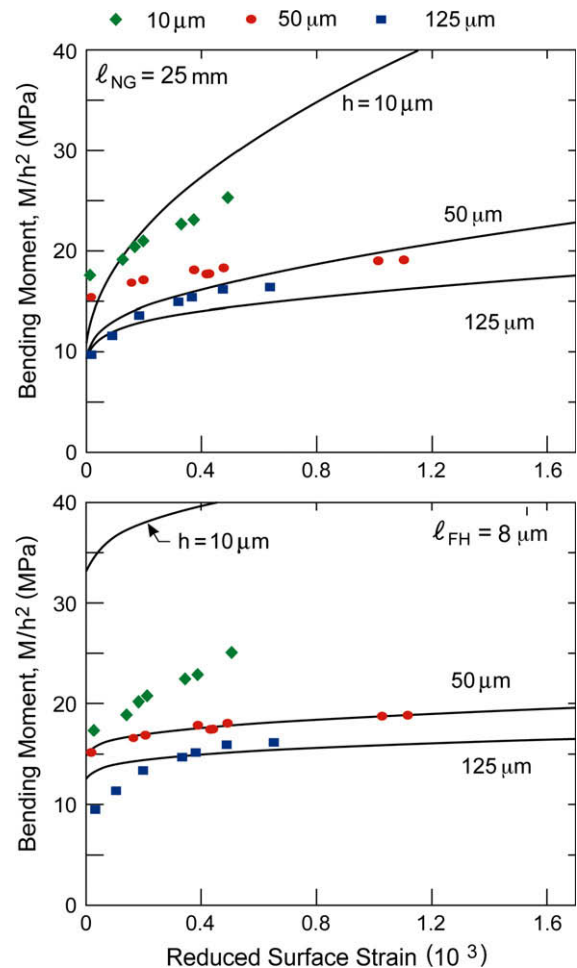


Fig. 7. Comparison between experimental data from Fig. 1 for three foils with grain size $g = 27 \mu\text{m}$ and theoretical predictions from Fig. 5: upper plot, NG; lower plot, FH.

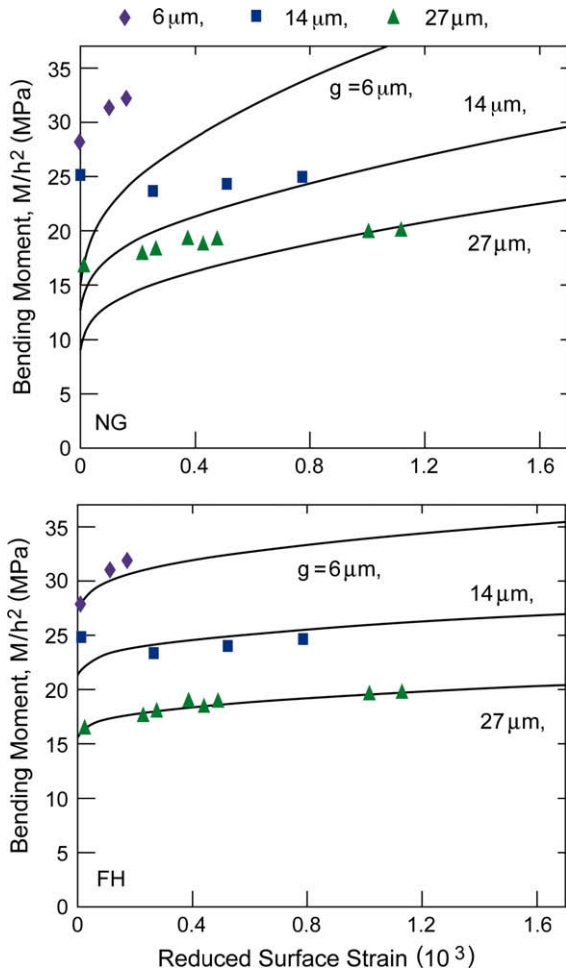


Fig. 8. Comparison between experimental data from Fig. 1 for three grain sizes for foils with thickness $h = 50 \mu\text{m}$, and theoretical predictions from Fig. 6: upper plot, NG; lower plot, FH.

are inadequate. Another is that a single comparison is insufficient to distinguish the respective models. Nevertheless, the discrepancies have motivated the introduction of a two-parameter FH model (described in Section 5) which achieves closer correspondence between measurement and theory.

For completeness, note that the FH theory with $\mu = 2$ (Appendix C) has the weakest correlation with the measurements (due to lowest-order strengthening proportional to $(\ell \varepsilon_p^*)^2$).

3.3. The approach to the size-independent limit

The lowest-order strengthening dependence on $\ell \varepsilon_p^*$ is exemplified by the appreciable body of Berkovitch nano-indentation data [4]. These data reveal that, as the depth of penetration d becomes large, the hardness H approaches the limit for large indents H_0 , in accordance with “square root” proportionality $[(H/H_0)^2 - 1 \propto \ell/d]$. The analog in bending is a plot of M^2 against $1/h$ at a fixed surface strain ($\varepsilon_s = 2\kappa/h$). The plot (Fig. 9) establishes that both the NG and the FH theories (with $\mu = 1$) are consistent with this

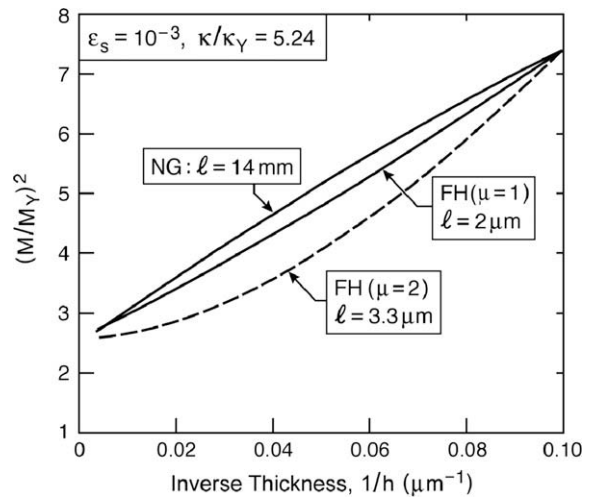


Fig. 9. A plot illustrating the predicted size dependence in bending with emphasis on the approach to the size-independent limit ($1/h \rightarrow 0$). This example was computed using uniaxial stress–strain data for the foil with $g = 27 \mu\text{m}$ at imposed curvature $\kappa/\kappa_Y = 5.24$ ($\varepsilon_s = 10^{-3}$) with size-independent limit $(M/M_Y)^2 = 2.6$. The length parameter for each theory was calibrated such that the predictions coincide with $(M/M_Y)^2 = 7.4$ at $\kappa/\kappa_Y = 5.24$ for foils with $h = 10 \mu\text{m}$ (at the right-hand side of the plot).

trend: a direct consequence of the lowest-order dependence of the formulations on $\ell \varepsilon_p^*$.

4. An illustration of the importance of a higher-order theory

The foregoing bending solutions have assumed that the plastic deformation at the surfaces is unconstrained (Appendix A). Suppose, instead, that dislocation motion is blocked by a thin passivation film, whereupon the plastic strain vanishes at the surfaces (Fig. 3) [9]. Such a boundary condition cannot be modeled by any lower-order theory. But a higher-order theory includes the possibility of specifying an additional boundary condition $\varepsilon_P = 0$ at the surfaces (Appendix A). The basis for the difference is that, in the lower-order theory, the gradient only affects the incremental moduli: otherwise, it involves conventional measures of the stress and strain. As a result, only conventional boundary conditions can be enforced. By contrast, any theory based on the plastic work is inherently higher-order, because the work depends on the strain and its gradient, and both must be retained as essential variables. There are two consequences: (i) the theory embraces additional boundary conditions; (ii) an additional stress-like quantity arises with dimensions stress \times length denoted by T . This new quantity is referred to as a “higher-order stress” or, in some contexts, as a couple or moment stress; T works through the strain gradient to generate the stored energy and dissipation associated with the GND (Appendix A). An illustration showing how T relates to material properties is presented in Appendix B, along with examples of parameters with similar dimensions familiar in dislocation theory.

The influence on the moment–surface strain relation predicted by FH is plotted in Fig. 10 for foils with grain

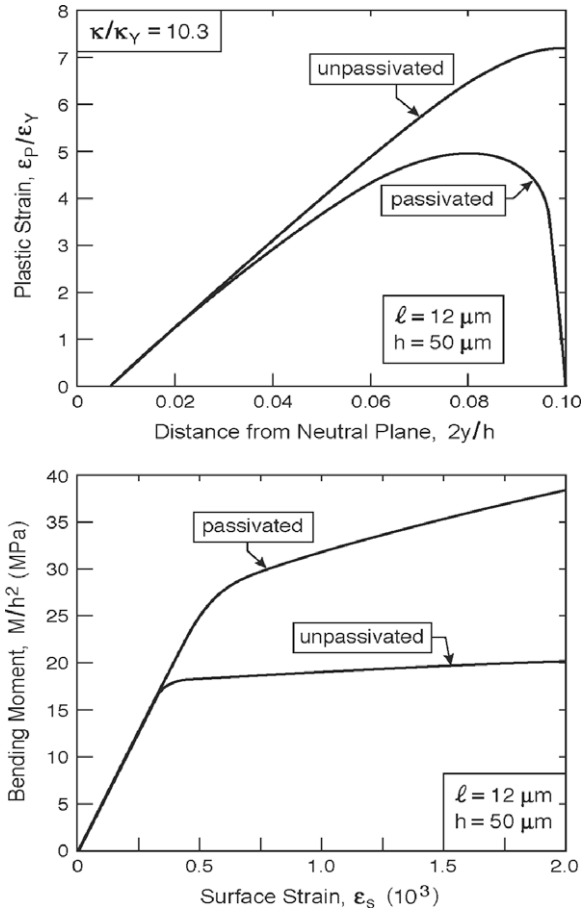


Fig. 10. The role of passivated surfaces, as predicted by FH theory with $\mu = 2$. The passivation layer blocks dislocations such that $\varepsilon_p = 0$ at the surfaces, but is otherwise assumed to have negligible thickness. There is no constraint on ε_p for the unpassivated surface, as in all the previous figures: lower figure, normalized moment vs surface strain ε_s ; upper figure, distribution of ε_p across the upper half of the foil at $\kappa/\kappa_Y = 10.3$.

size $g = 27 \mu\text{m}$ and thickness $h = 50 \mu\text{m}$. The corresponding distributions of effective plastic strain (at $\kappa/\kappa_Y = 10.3$) are also shown in Fig. 10. Note that the effect of passivation in bending is large because yielding starts at the surfaces where plasticity is severely constrained.

It is re-emphasized that no conventional plasticity theory or lower-order theory of any kind could distinguish between passivated and unpassivated surfaces. The higher-order formulation provides the flexibility needed to specify boundary conditions not encompassed by lower-order theories. This flexibility is illustrated through schematics of the spatial organizations of the GND in bending (Fig. 11) along with the associated continuum plastic strain distributions, $\varepsilon_{11}^p(y)$ (cf., Fig. 10). For these distributions, the dislocation density is $\rho_{\text{GND}} = b^{-1} d\varepsilon_{11}^p/dy$. The dislocations exit through an unpassivated surface (a dislocation pile up cannot be sustained), whereupon, at the surface, $\rho_{\text{GND}} = b^{-1} d\varepsilon_{11}^p/dy = 0$, and T vanishes. By contrast, dislocations pile up at the passivated surface, with non-zero ρ_{GND} and T , while the plastic strain vanishes. The mathematical structure of the higher-order theory, including the definition of T and how it relates to the boundary conditions, is presented in Appendix A.

5. Formulation with a strain-dependent length scale

An attractive feature of both the NG and FH models is that they require the specification of only a single material length parameter in addition to the standard inputs to conventional J_2 plasticity theory (Appendix A). As evident from the comparison between predictions and the data in Figs. 7 and 8, this simplicity also constrains the ability of the theory to reproduce measurements. Both models can incorporate additional parameters, permitting greater flexibility. The process is illustrated for the FH model by generalizing Eq. (7), through a strain-dependent length scale, according to

$$E_p = \varepsilon_p + \ell(\varepsilon_p)\varepsilon_p^* \quad (14)$$

as described in Appendix A. The specific example in Fig. 12 for the foil with $g = 27 \mu\text{m}$ and $h = 50 \mu\text{m}$ introduces two parameters, ℓ_0 and a_0 , as

$$\ell(\varepsilon_p) = \ell_0[1 + a_0(\varepsilon_p/\varepsilon_Y)] \quad (15)$$

where a_0 clearly invokes a linear dependence of the length scale on the plastic strain. By decreasing the initial strengthening and increasing the rate of hardening, the parameters chosen in Fig. 12 clearly give a better fit to the data. While adding another parameter is hardly desirable, nevertheless it is comforting to establish that the theories can be extended in a relatively straightforward manner to replicate more closely a wide range of measurements incorporating strain gradients.

6. Interpretation of the length scale

Strain gradient theories have not been comprehensively embraced for several reasons. Most importantly, the ambiguities surrounding the length parameters that emerge upon fitting predictions from different theories to measurements are a source of confusion which the foregoing bending tests highlight. A further hindrance is the lack of clarity associated with the interpretation of the theories within an explicit dislocation dynamics context [28]. The following discussion provides rudimentary connections between the length scales and dislocation-based phenomena.

Before proceeding, the authors recall that both the NG and FH formulations appeal to GND as the source of the size effects, and both relate the density of GND to the plastic strain gradient in essentially the same manner (see Appendix A), motivated by explicit connections between the density of GND and gradients of plastic strain in single crystal theory [14,29]. Divergences between the two theories arise from the manner in which the strain and the strain gradient are combined, as expounded in Section 2, leading to the huge differences between the length parameters. Neither theory makes the distinction that the GND induced by the strain gradients are closely correlated, whereas the SSD are relatively uncorrelated. Moreover, neither theory accounts for interactions among the dislocation categories.

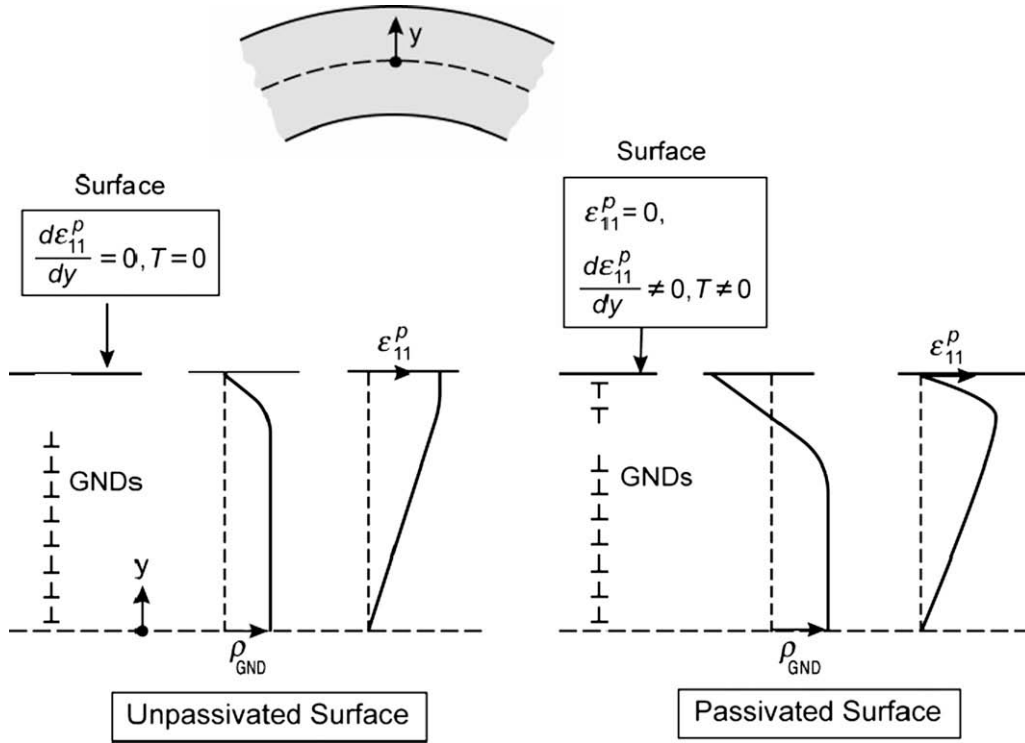


Fig. 11. Schematic of dislocation and plastic strain distributions in bending for foils with unpassivated and passivated surfaces.

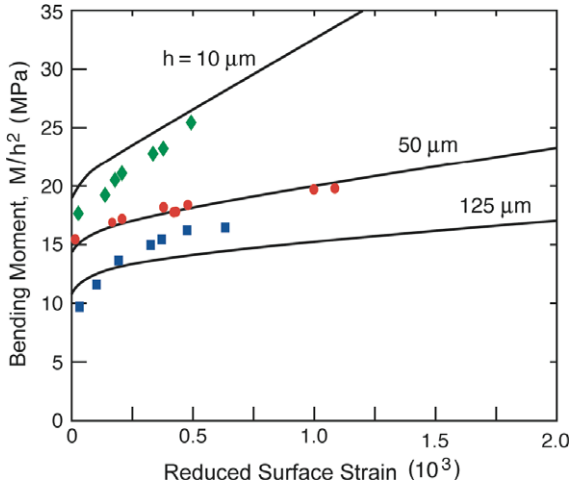


Fig. 12. Prediction from FH theory incorporating a strain-dependent length parameter, $\ell(\varepsilon_p) = \ell_0(1 + a_0(\varepsilon_p/\varepsilon_Y))$. The values $\ell_0 = 2 \mu\text{m}$ and $a_0 = 0.2$ were chosen both to fit the data for the foil with $h = 50 \mu\text{m}$ at $\varepsilon_R = 10^{-3}$ and to represent better the initial increase in strength and hardening of the foil with $h = 10 \mu\text{m}$.

The connection in Eq. (3), $\ell_{\text{NG}} = \chi(G/\sigma_Y)^2 \alpha^2 b$, underpins the physical basis of the NG formulation [4]. If the yield strength is set by the current density of SSD, Taylor hardening gives $\sigma_Y \approx Gb\sqrt{\rho_{\text{SSD}}} \approx Gb/s$, with s representing an effective spacing between obstacles (dislocation cell size or precipitate spacing). Neglecting numerical factors

$$\ell_{\text{NG}} \approx s^2/b \quad (16)$$

The spacing estimated from Eq. (16) in conjunction with the inferred length scale $\ell_{\text{NG}} = 25 \mu\text{m}$ is credible: $s \approx 2.5 \mu\text{m}$. Nevertheless, the previously noted discrepancy between α as a fitting factor and its interpretation as the Taylor hardening coefficient persists. For example, for the bending measurements at $g = 27 \mu\text{m}$ ($\sigma_Y = 42 \text{ MPa}$), formula (3) predicts $\ell_{\text{NG}} = 2.8 \text{ mm}$ when the usual choice of α is used ($\alpha = 0.4$); much smaller than $\ell_{\text{NG}} = 25 \text{ mm}$ (with $\alpha = 1.13$) inferred by reproducing the data.

The clearest microscopic interpretation of ℓ_{FH} emerges upon letting $\Delta\rho_{\text{SSD}}$ and $\Delta\rho_{\text{GND}}$ be the densities of mobile SSD and GND associated with the plastic strain ε_p and gradient ε_p^* , respectively, and \bar{d} the average distance they travel (again set by dislocation cell size or precipitate spacing). The plastic dissipation is

$$U_p \approx \sigma_Y(\Delta\rho_{\text{SSD}}b\bar{d} + \Delta\rho_{\text{GND}}b\bar{d}) \quad (17)$$

$$\text{Given that } \varepsilon_p \approx \Delta\rho_{\text{SSD}}b\bar{d} \text{ and } \varepsilon_p^* \approx \Delta\rho_{\text{GND}}b$$

$$U_p \approx \sigma_Y(\varepsilon_p + \bar{d}\varepsilon_p^*). \quad (18)$$

Based on Eqs. (5) and (6)

$$U_p \approx \sigma_Y E_p = \sigma_Y(\varepsilon_p + \ell_{\text{FH}}\varepsilon_p^*)$$

The identity $\ell_{\text{FH}} \approx \bar{d}$ implies that the length scale is determined by the average distance between obstacles. This outcome is consistent with the statement that ℓ_{FH} sets the scale of the gradient, whereupon the motions of the GND and SSD contribute equally to the dissipation. It is also notable that, for all the cases interpreted using FH, there is a strong inverse correlation between ℓ_{FH} and the yield strain

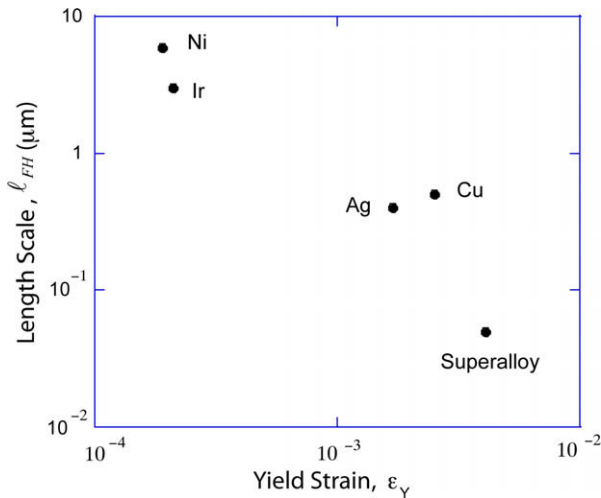


Fig. 13. A plot of the length scale l_{FH} against the size-independent tensile yield strain. The length scale was ascertained by FH theory using indentation data for Ir [3], a superalloy [30], copper [5] and silver [2], together with the present finding for bending of Ni foils.

(Fig. 13). That such a correlation exists is consistent with the proposed dependence of l_{FH} on the distance moved by the dislocations, which, in turn, dictates the plastic strain. Similar trends can be ascertained from the NG theory provided that the originally conceived notion that α is constant be abandoned. Indeed, fitting to the theory reveals that $\alpha \approx 1$ for the low yield strain Ni foils in bending, $\alpha \approx 0.3$ for indentation of Ag and Cu, and $\alpha \approx 0.05$ for indentation of the high-strength superalloy [30].

The two microscopic interpretations of the length scale are not necessarily in conflict. Both estimates are within the realm of possibility. Recall that, instead, the important divergences between the formulations are twofold: (i) the strong strain dependence of l_{NG} contrasts with the relative strain invariance of l_{FH} ; and (ii) the size effect in the NG theory involves increases in rates of hardening, with little initial strength increase, whereas the FH theory predicts a substantial increase in yield strength with a smaller increase in the rate of strain hardening. The strong strain dependence of l_{NG} can also be problematic. For example, indentation tests are one of the simplest and most robust ways to determine the material length parameter. However, unless the strain dependence of the fitting factor α in Eq. (3) were determined independently, it would not be possible to use l_{NG} ascertained from indentation tests to predict the small strain bending of foils.

7. Concluding remarks

By pursuing the two prominent strain gradient theories within the context of a benchmark problem, simple bending, the following important differences were highlighted. The strong strain dependence of l_{NG} contrasts with the relative strain invariance of l_{FH} . The size effect in NG theory involves an increase in hardening, with little effect on initial yield: whereas FH theory predicts a substantial increase in

yield strength with only a small increase in strain hardening. Both theories deviate from the bending measurements but, in a broader context, other measurements reveal a larger effect of the gradient on yielding than on strain hardening. By adding an extra coefficient, the theories can be adjusted to attain levels of strengthening and strain hardening that more closely match the measurements. This capability was illustrated for the FH theory.

The length scales inferred by fitting to experimental measurements have the following rudimentary connections to dislocation phenomena. The strengthening in the NG theory is governed by the spacing between the GND. The FH theory is based on the plastic dissipation, enabling the length scale to be related to the average distance between obstacles moved by the GND. This correlation is the basis for the inverse dependence of l_{FH} on the yield strain.

The difference between lower-order (conventional NG) and higher-order (FH) theory was emphasized and illustrated by the example of surface passivated foils in bending. The distinction is that the low-order theory is restricted in terms of the boundary conditions that can be imposed, excluding the solution of various important problems. The higher-order theory does not have this restriction, because it introduces a new quantity (with dimensions stress \times length) governing the plastic work within the strain gradient: analogous to the dissipation within dislocation pile ups. Accordingly, higher-order theory can solve problems involving locations where the plastic strain is zero owing to the blockage of dislocations.

The version of FH pursued in the present paper used the linear summation of the plastic strains and their gradients ($\mu = 1$) because this choice correlates with well-established “square root” size scaling trends found in hardness and other tests. Most prior applications conducted using FH used $\mu = 2$, largely because the numerical implementation is most straightforward for this case. However, given the disconnect between this version and scaling trends, it is proposed that it be abandoned or restricted to the mid-range of the size effect. The ensuing challenge is that, to progress further with the linear version of FH, non-standard numerical methods must be devised to obtain solutions to generalized problems.

The uncertainties that remain from this assessment suggest continued critical evaluation of the basic formulations with input guided by fundamentals of dislocation mechanics. Further progress requires better experimental data for a range of materials using bending, torsion and shear as benchmarks. While the forgoing bending data represent an advance over prior data, its limitations in spanning the relevant range of foil thickness and strain are nevertheless apparent. Further experimental data, such as those in Fig. 3 (comparing the behavior of films with and without passivation) [9] but applied to thin wires in torsion and foils in bending, would provide an especially critical assessment of the higher-order formulation. In turn, these aspects are closely tied to the thickness of boundary layers and shear

bands, only amenable to characterization by a higher-order formulation.

Acknowledgments

The authors are indebted to a critique of the original draft of the paper supplied by a reviewer and to suggestions from H. Gao, Y. Huang and W.D. Nix.

Appendix A. Synopsis of low- and high-order theories

Within the framework of single crystal plasticity, explicit connections exist between densities of GND and the gradients of plastic strain [14,29]. The starting point for all phenomenological isotropic theories is the definition of a measure of the gradient of plastic strains ε_p^* . The FH formulation uses the most general measure based on the three quadratic invariants $I_i (i = 1, 3)$ of the gradients $\varepsilon_{ij,k}^p$:

$$\sqrt{\ell_1^2 I_1 + \ell_2^2 I_2 + \ell_3^2 I_3} \equiv \ell_{\text{FH}} \varepsilon_p^* \quad (19)$$

Definitions of these invariants, which are non-negative and have dimensions (length)⁻², are given in [14,15]. Three length parameters, $\ell_i (i = 1, 3)$, arise. For bending in plane strain

$$\sqrt{\ell_1^2 I_1 + \ell_2^2 I_2 + \ell_3^2 I_3} = \sqrt{\frac{4}{5} \ell_1^2 + \ell_2^2 + \frac{6}{5} \ell_3^2 |\varepsilon_p'|} \equiv \ell_{\text{FH}} \varepsilon_p^* \quad (20)$$

The NG formulation [16,17] also employs Eq. (19), but the number of length parameters is reduced to one by fixing the ratios as $\ell_1 = \ell_2 = \ell_3$.¹ The measure of plastic strain gradients is taken as

$$\eta_p = (1/2) \sqrt{I_1 + I_2 + I_3} \quad (21)$$

and the contribution to the flows stress in Eq. (2) is $\ell \eta_p$. In plane strain bending

$$\ell \eta_p = \ell \frac{\sqrt{3}}{2} |\varepsilon_p'| \equiv \ell_{\text{NG}} \varepsilon_p^* \quad (22)$$

Note that the length parameter ℓ , as defined by Gao et al. [16,17], is $2/\sqrt{3}$ times the length ℓ_{NG} employed in the present paper.

Distinctions between lower- and higher-order gradient theories are illustrated within the context of pure bending. For an elastically incompressible material in plane strain and subject to $\kappa > 0$, the relations introduced earlier hold for $y \geq 0$:

$$\varepsilon_{11} \equiv \varepsilon = \kappa y, \quad \varepsilon_p = 2\varepsilon_p^p / \sqrt{3}, \quad \varepsilon_p^* = |d\varepsilon_p/dy| \quad (23)$$

In both formulations, the conventional stresses are given by

$$\sigma_{11} = (4/3)E(\varepsilon_{11} - \varepsilon_{11}^p) = (4/3)E(\kappa y - \sqrt{3}\varepsilon_p/2) \quad (24)$$

with $\sigma_{33} = \sigma_{11}/2$, and the effective stress is $\sigma_e = \sqrt{3}\sigma_{11}/2$. Because the two non-zero stress components are functions only of y , the conventional equilibrium equations, $\sigma_{ij,j} = 0$, are identically satisfied.

A.1. Lower-order gradient theory: NG as an example

Most applications of NG have made use of the lower-order theory [18] (albeit that higher-order versions have been proposed [16,17]). For problems more complicated than pure bending, a numerical technique (typically finite elements) is needed to obtain solutions for the stresses, based on the incremental equations governing stress–strain, equilibrium and strain–displacement. These equations have the same form as conventional plasticity, except that the incremental moduli relating stress and strain increments in the plastically deforming regions would have an additional dependence on the gradient of plastic strain. The effects of the gradients are innocuous in that they do not fundamentally alter the structure of conventional plasticity [31]. In particular, they do not require, or permit, specification of extra boundary conditions, such as the constraint on plastic flow imposed by passivation described in Section 4.

Bending subject to increasing κ is sufficiently simple that the following direct approach is the most straightforward way to produce the solution. Let $\varepsilon_Y = \sigma_Y/E$ be the initial tensile yield strain and $\kappa_Y = \sqrt{3}\varepsilon_Y/h$ be the curvature at which yielding starts at the surface ($y = h/2$). When $\kappa > \kappa_Y$, the region $y \leq Y \equiv \sqrt{3}\varepsilon_Y/(2\kappa)$ is elastic ($\varepsilon_p = 0$), while yielding ($\varepsilon_p \geq 0$) occurs for $y > Y$. By Eq. (24)

$$\varepsilon_{11}^p \equiv \frac{\sqrt{3}}{2} \varepsilon_p = \kappa y - \frac{\sqrt{3}}{2} \frac{\sigma_Y}{E} \sqrt{f(\varepsilon_p)^2 + \ell_{\text{NG}} \varepsilon_p^*} \quad (y \geq 0) \quad (25)$$

where the gradient-enhanced NG flow stress σ_e from Eq. (2) is introduced. Solving for $\varepsilon_p^* = d\varepsilon_p/dy$ and introducing $\bar{\varepsilon}_p = \varepsilon_p/\varepsilon_Y$ and $\eta = 2y/h$ gives a first-order ordinary differential equation for $\bar{\varepsilon}_p$:

$$\frac{d\bar{\varepsilon}_p}{d\eta} = \frac{1}{(2\ell_{\text{NG}}/h)\varepsilon_Y} \left[\left(\frac{\kappa}{\kappa_Y} \eta - \bar{\varepsilon}_p \right)^2 - f(\bar{\varepsilon}_p)^2 \right] \quad (26)$$

The only boundary condition that can be enforced is the requirement that $\bar{\varepsilon}_p = 0$ at the elastic–plastic boundary at $y = Y$ ($\eta = \eta_Y \equiv \kappa_Y/\kappa$). It is not possible to constrain the plastic strain additionally at the surface. The results presented in the body of the paper are obtained by integrating Eq. (26) numerically from η_Y to the surface at $\eta = 1$. For $\kappa > \kappa_Y$, the moment/length is

$$M = 2 \int_0^{h/2} \sigma_{11} y dy = M_Y \left\{ \left(\frac{\kappa_Y}{\kappa} \right)^2 + 3 \int_{\eta_Y}^1 \left(\frac{\kappa}{\kappa_Y} \eta - \bar{\varepsilon}_p \right) \eta d\eta \right\} \quad (27)$$

where $M_Y = \sigma_Y h^2 / (3\sqrt{3})$ is the moment/length at the onset of plastic yielding. The equation governing the plastic

¹ This restriction is in accord with the fact that the three lengths are not associated with distinct physical mechanisms. While a single length reduces somewhat the flexibility to fit data from different types of deformations (e.g., wire torsion and indentation [5]), the restriction taking the three parameters to be equal is a good compromise as discussed in Ref. [17].

strain distribution for conventional plasticity is obtained from Eq. (26) in the limit $\ell_{NG} \rightarrow 0$, i.e., $\bar{\epsilon}_p + f(\bar{\epsilon}_p) = (\kappa/\kappa_Y)\eta$.

A.2. Higher order gradient theory: FH as an example

The FH formulation employs the plastic work required to deform a material element $U_P(E_P)$, with E_P given by Eq. (6). Attention is again focused on the upper half of the beam. For the deformation theory formulation, the energy/length required to deform the beam to curvature $\kappa > \kappa_Y$ is

$$\begin{aligned} \Phi &= 2 \int_0^{h/2} \left[\frac{1}{2} \sigma_{11} \epsilon_{11}^e + U_P(E_P) \right] dy \\ &= 2 \int_0^{h/2} \left[\frac{2}{3} E \left(\kappa y - \frac{\sqrt{3}}{2} \epsilon_p \right)^2 + U_P(E_P) \right] dy \end{aligned} \tag{28}$$

The first term is the elastic energy and the second is the plastic work. For the case of no constraint on plastic flow at the surface, the plastic strain distribution $\epsilon_p(y)$ is determined by minimizing Φ with respect to all continuous distributions ϵ_p that vanish for $y \leq Y$ and are non-negative for $y > Y$. The first variation in Φ with respect to ϵ_p is

$$\begin{aligned} \delta\Phi &= 2 \int_Y^{h/2} \left[-\frac{2}{\sqrt{3}} E \left(\kappa y - \frac{\sqrt{3}}{2} \epsilon_p \right) \delta\epsilon_p + \frac{\partial U_P}{\partial \epsilon_p} \delta\epsilon_p \right. \\ &\quad \left. + \frac{\partial U_P}{\partial \epsilon_p'} \delta\epsilon_p' \right] dy \\ &= 2 \int_Y^{h/2} \left[-\sigma_e \delta\epsilon_p + \frac{\partial U_P}{\partial \epsilon_p} \delta\epsilon_p + \frac{\partial U_P}{\partial \epsilon_p'} \delta\epsilon_p' \right] dy \end{aligned} \tag{29}$$

with $(\prime) = d()/dy$. The inevitable consequence of the dependence of energy on the gradient of plastic strain is that a new quantity with dimensions stress \times length ($N\ m^{-1}$) arises, not present in conventional plasticity. This parameter, designated T , is the work conjugate to the plastic strain gradient ϵ_p' and identified as

$$T = \partial U_P / \partial \epsilon_p' \tag{30}$$

That is, $T\delta\epsilon_p'$ is interpreted as the contribution to the plastic work increment due to the GND. Integrating the third term in Eq. (29) by parts gives

$$\delta\Phi = 2 \int_Y^{h/2} [-\sigma_e + Q - T'] \delta\epsilon_p dy + 2[T\delta\epsilon_p]_Y^{h/2} \tag{31}$$

where $Q = \partial U_P / \partial \epsilon_p$. The requirement that $\delta\Phi = 0$ for all $\delta\epsilon_p$, satisfying $\epsilon_p = 0$ at $y = Y$, provides the equilibrium equation for the higher-order stress and the extra boundary condition at the surface:

$$T' - Q + \sigma_e = 0 \quad \text{on } Y \leq y \leq h/2 \tag{32}$$

and

$$T = 0 \quad \text{at } y = h/2 \tag{33}$$

For the case where plastic flow is blocked at the surface, the admissible distributions must be additionally constrained

such that $\epsilon_p = 0$ at $y = h/2$; then T does not vanish at the surface. Because $d\Phi = Mdk$, one can show that M is again given by Eq. (27).

In summary, for bending in the lower-order theory, a first-order, ordinary differential equation governs ϵ_p , and the only condition that can be enforced is that ϵ_p vanish at the elastic–plastic boundary. The equilibrium equation for the higher-order theory, Eq. (32), when expressed in terms of ϵ_p , becomes a second-order, ordinary differential equation. Boundary conditions at both the elastic–plastic boundary and at the surface can be imposed, modeling either blocked or unblocked dislocation motion (or even intermediate conditions with further embellishment [23]).

Inclusion of a strain dependence of the length parameter $\ell_{FH}(\epsilon_p)$, as illustrated by Eq. (15), creates no difficulties. The dependence $\ell_{FH}(\epsilon_p)$ appears in E_P and in $U_P(E_P)$ and is directly accounted for in the quantities $Q = \partial U_P / \partial \epsilon_p$ and $T = \partial U_P / \partial \epsilon_p'$. In other words, the additional flexibility afforded by the strain-dependent length parameter creates no theoretical or computational obstacles [32]. The results presented in the figures were obtained by minimizing Φ with respect to $\epsilon_p(y)$ subject to the constraints enumerated above, with

$$U_P(E_P) \equiv \int_0^{E_P} \sigma_e d\epsilon_p = \sigma_Y \left[E_P + \frac{\lambda \epsilon_Y}{(N+1)} \left(\frac{E_P}{\epsilon_Y} \right)^{N+1} \right] \tag{34}$$

The minimization process was implemented numerically. For $\mu > 1$, various methods can be used, including a one-dimensional finite element method with a piecewise linear approximation to $\epsilon_p(y)$. For $\mu = 1$, the choice of methods narrows, because the minimum is not necessarily analytic, and the solution for $\epsilon_p(y)$ can have discontinuities in its first derivative. In the present paper, the interval $Y \leq y \leq h/2$ was subdivided into equal elements, a piecewise linear approximation to $\epsilon_p(y)$ was used, and the minimum of Φ was obtained using a standard routine for constrained optimization. To apply this formulation to two- and three-dimensional problems, efforts will have to be made to identify efficient and robust numerical solution methods.

Appendix B. An explicit illustration of the higher-order stress T

The origin of the higher-order stress T is illustrated for the uniform rectangular array of edge dislocations in Fig. 14 associated with pure bending of a beam of thickness h . The dislocation array produces a macroscopic curvature, $\kappa = b/sd$, and uniform plastic strain gradient, $\epsilon_p' = \kappa = b/sd$. All the dislocations are geometrically necessary. The beam is unloaded with traction-free upper and lower surfaces and no net axial force and bending moment. The plane strain elasticity problem for the stress distribution in the infinitely long beam can be solved exactly [33]. The stress acting in the horizontal direction σ_{xx} on a vertical plane midway between any two columns of dislocations is plotted in Fig. 14, for an example, with 15 dislocations

across the beam thickness. The stress oscillates with the scale of the dislocation spacing, modified in the vicinity of the free surfaces.

In this example, only the elastic energy associated with the dislocations is considered. Dissipation associated with GND formation and motion is neglected. The elastic energy/volume U scales with the dislocation energy/length ($\propto Eb^2$) divided by the area/dislocation (s/d). Specifically, with c as the radius of the dislocation core, the functional form for U for dislocations away from the free surface is

$$U = \frac{Eb^2}{(1-\nu^2)sd} f\left(\frac{c}{d}, \frac{s}{d}, \nu\right) \quad (35)$$

The elastic energy was computed numerically for various values of the arguments of Eq. (35). As an example, with $c/d = 10^{-4}$ and $\nu = 1/3$, U is accurately approximated by

$$U = \frac{Eb^2}{(1-\nu^2)sd} \left[2.80 + 0.42 \frac{s}{d} \right], \quad \text{for } s/d \geq 1, \quad (36)$$

If the beam contains many dislocations across its thickness, U can be regarded as the continuum average of the energy/volume. Moreover, Eq. (35) can be rewritten in terms of the plastic strain gradient as

$$U = \frac{Eb}{(1-\nu^2)} \left[2.80 \epsilon'_p + 0.42 \frac{b}{d^2} \right] \quad (37)$$

Suppose $\epsilon'_p = b/sd$ is increased by decreasing the vertical spacing between the dislocations s , with d held fixed. Recalling the definition of T in Eq. (30),

$$T = \frac{\partial U}{\partial \epsilon'_p} = 2.80 \frac{Eb}{(1-\nu^2)}, \quad \text{for } s/d \geq 1 \quad (38)$$

In summary, this idealized example illustrates that the energy associated with the array of GND depends on the plastic strain gradient, and not on the plastic strain. Consequently, the increment of the energy/volume, $dU = T d\epsilon'_p$, naturally involves a parameter T , with dimensions stress \times length. Mathematically, T is work conjugate to $d\epsilon'_p$.

It is emphasized that the stored elastic energy of the GND in this example represents their free energy. The dissipative contribution to the work of moving them has not been considered. Generally, the free energy contribution only becomes dominant at very small dislocation spacing.

A parameter with the same dimensions (stress \times length) familiar in dislocation theory is the force on a dislocation (per unit length): namely, the product of the shear flow stress and the Burgers vector. The elastic energy of a dislocation per unit area of slip plane also has the same dimensions.

Appendix C. The exponent in FH theory

The FH formulation employing the effective plastic strain (Eq. (7)) with exponent $\mu = 1$ is used in the body of the paper because it captures the size dependence with more fidelity than the more widely used version with $\mu = 2$. The original studies of Fleck and Hutchinson [14,15] and others favored $\mu = 2$ over $\mu = 1$ primarily on mathematical grounds and not on the basis of physical considerations. The following difficulties emerge when using the choice $\mu = 2$. A length parameter $\ell_{FH} = 12 \mu\text{m}$ fits the data for the foil with grain size $g = 27 \mu\text{m}$ and thickness $h = 50 \mu\text{m}$. However, the behavior predicted for the other two thicknesses is poorly represented and, in particular, the bending moment of the thinnest foil is substantially overestimated. Conversely, if ℓ_{FH} had been chosen to fit the data for the thinnest foil, the strengthening for the thicker foils would be underestimated. As already noted, this inadequacy arises because, when the gradient contribution is relatively small, the version with $\mu = 2$ predicts strength increases on the order of $(\ell \epsilon'_p)^2$, while the NG formulation and the FH version with $\mu = 1$ both predict strengthening of order $\ell \epsilon'_p$.

References

- [1] Stelmashenko NA, Walls MG, Brown LM, Minman YV. Acta Met Mater 1993;41:2855.
- [2] Ma Q, Clarke DR. J Mater Res 1995;10:853.
- [3] Swadener JG, George EP, Pharr GM. J Mech Phys Solids 2002;50:681.

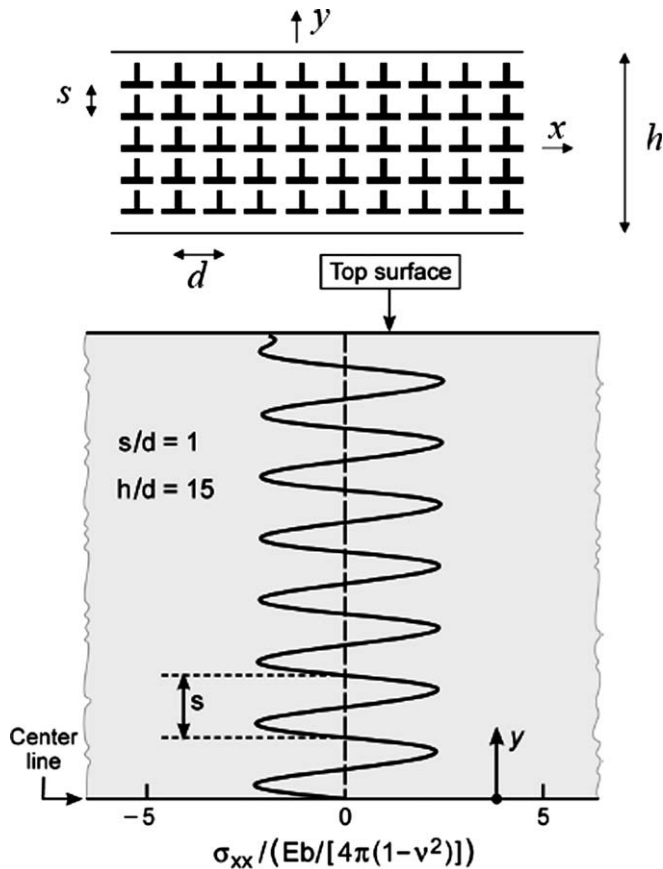


Fig. 14. Horizontal stress distribution halfway between dislocation columns in the upper half of a slab containing a uniform rectangular array of dislocations. The slab is subject to pure bending due to the array with no external loads.

- [4] Nix WD, Gao H. *J Mech Phys Solids* 1998;46:411.
- [5] Begley MR, Hutchinson JW. *J Mech Phys Solids* 1998;46:2049.
- [6] Huang Y, Xue Z, Gao H, Nix WD, Xia ZC. *J Mater Res* 2000;15:1786.
- [7] Fleck NA, Muller GM, Ashby MF, Hutchinson JW. *Acta Met Mater* 1994;42:475.
- [8] Stolken JS, Evans AG. *Acta Mater* 1998;46:5109.
- [9] Xiang Y, Vlassak JJ. *Acta Mater* 2006;54:5449.
- [10] Petch NJJ. *Iron Steel Inst* 1953;174:25.
- [11] Lloyd D. *J Int Mater Rev* 1994;39:1.
- [12] Ashby MF. *Phil Mag* 1970;21:399.
- [13] Aifantis EC. *J Eng Mater Tech* 1984;106:326.
- [14] Fleck NA, Hutchinson JW. *Adv Appl Mech* 1997;33:295.
- [15] Fleck NA, Hutchinson JW. *J Mech Phys Solids* 2001;49:2245.
- [16] Gao H, Huang Y, Nix WD, Hutchinson JW. *J Mech Phys Solids* 1999;47:1239.
- [17] Huang Y, Gao H, Nix WD, Hutchinson JW. *J Mech Phys Solids* 2000;48:99.
- [18] Huang Y, Qu S, Hwang KC, Li M, Gao H. *Int J Plasticity* 2004;20:753.
- [19] Ehrler B, Hou XD, Zhu TT, P'ng KMY, Walker CJ, Bushby AJ, et al. *Phil Mag* 2008;88:3043.
- [20] Ebrahimi F, Bourne GR, Kelly MS, Mathews TE. *Nanostruct Mater* 1999;11:343.
- [21] Hansen N. *Scripta Mater* 2004;51:801.
- [22] Gudmundson P. *J Mech Phys Solids* 2004;52:1379.
- [23] Aifantis K, Soer W, De Hosson J, Willis J R. *Acta Mater* 2006;54:5077.
- [24] Gurtin ME. *Int J Plasticity* 2003;19:47.
- [25] Gurtin ME. *J Mech Phys Solids* 2002;50:5.
- [26] Evers LP, Brekelmans WAM, Geers MGD. *J Mech Phys Solids* 2004;52:2379.
- [27] Cleveringa HHM, van der Giessen E, Needleman A. *Acta Mater* 1997;45:3163.
- [28] Mughrabi H. *Mat Sci Eng A* 2004;387–389:209.
- [29] Arsenlis A, Parks D M. *Acta Mater* 1999;47:1597.
- [30] Hemker KJ, Mendis BG, Eberl C. *Mater Sci Eng A* 2008;483–484:727 (Indentation data supplied by private communication).
- [31] Bassani JL. *J Mech Phys Solids* 2001;49:1983.
- [32] Voyiadjis GZ, Abu Al-Rub RK. *Int J Solids Struct* 2005;42:3998.
- [33] Hutchinson JW, unpublished work.